Magnetic Resonance in Medicine 67:1694–1702 (2012)

Motion Correction and Registration of High *b*-Value Diffusion Weighted Images

Shani Ben-Amitay,[1] Derek K. Jones,[2,3] and Yaniv Assaf[1]*

It has been suggested that, high *b*-value diffusion weighted MRI improves the sensitivity and specificity of these images to tissue microstructure when compared with "clinical" *b*-value diffusion weighted MRI ($b \approx 1000$ s/mm^2). However, it suffers from poor signal to noise ratio - leading to longer acquisition times and therefore more motion artifacts. Together with the orientational sensitivity of the diffusion weighted MRI signal, the contrast at different *b*-values and different gradient directions is significantly different. These features of high *b*-value diffusion images preclude the ability to perform conventional image-registration-based motion/distortion correction. Here, we suggest a framework based on both experimental data (diffusion tensor MRI) and simulations (using the composite hindered and restricted model of diffusion framework) to correct the motion induced misalignments and artifacts of high *b*-value diffusion weighted MRI. This approach was evaluated using visual assessment of the registered diffusion weighted MRI and the composite hindered and restricted model of diffusion analysis results, as well as residual analysis to assess the quality of the composite hindered and restricted model of diffusion fitting. Both qualitative and quantitative results demonstrate an improvement in fitting the data to the composite hindered and restricted model of diffusion model following the suggested registration framework, thereby, addressing a long-standing problem and making the correction of motion/distortions in data collected at high *b*-values feasible for the first time. Magn Reson Med 67:1694–1702, 2012. © 2011 Wiley Periodicals, Inc.

Key words: high *b*-value; motion; registration; diffusion weighted MRI; white matter

High *b*-value diffusion MR imaging provides an enhanced contrast toward different cellular components (1,2) when compared with "clinical" diffusion MRI ($b \approx 1000$ s/mm^2). Combined with an appropriate model, the analysis of low and high *b*-value diffusion images may provide a comprehensive tissue characterization, enabling improved sensitivity and specificity of diffusion weighted MRI (DW-MRI) to healthy tissue microstructure and subtle pathology, especially in white matter (3,4).

Diffusion tensor MRI (DT-MRI) is a well-accepted framework for analysis of diffusion-weighted images (measured at low *b*-values up to ~ 1500 s/mm^2) and is mainly used to characterize white matter microstructure (5,6) and, by following the direction of greatest apparent diffusivity in each voxel, allows the reconstruction of three-dimensional fiber tracts (7). However, the resulting DT-MRI parameters represent an average of the diffusion properties in each voxel and in areas of intra-voxel heterogeneity, e.g., cerebrospinal fluid (CSF) or gray matter interfaces, affected by partial volume contamination, DT-MRI can fail to reveal the real microstructural properties of the tissue of interest (usually the white matter). DT-MRI's inability to resolve crossing fibers stems from the constraints of the tensor model, which assumes a single unimodal gaussian diffusion displacement profile (8). Q-space imaging (4,9), diffusion spectrum magnetic resonance imaging (DSI) (10), hybrid imaging (11), and the composite hindered and restricted model of diffusion (CHARMED) (3) are alternative models to DT-MRI that use both low and high *b*-value diffusion weighted data. These approaches overcome the major limitation of DT-MRI by using various nonmono-exponential attenuation models to infer on tissue microstructure. Using such methodologies, it is possible to extract physical and geometrical parameters regarding the orientation, diffusivity, and fractional volume for each of the components of the fiber system that contribute to the diffusion-weighted signal, allowing resolution of crossing fibers.

Despite the advantages conferred through high *b*-value diffusion imaging, the signal loss is much higher than in DT-MRI. Consequently, it suffers from poor signal to noise ratio, which is compensated for by lowering the resolution and/or collecting more data—leading to long acquisition times. This presents a serious challenge, even to the most motivated of volunteers, to remain perfectly still in the scanner while the entire set of DW-MR images is collected.

The most frequently adopted approach to correct for motion is to use image registration techniques to coregister each diffusion-weighted image to a reference image (usually the first $b = 0$ s/mm^2 image collected). Given the orientational sensitivity of the DW-MRI signal, cost-functions such as crosscorrelation and least-squares—used for intra-modal coregistration, are ineffective—and cost-functions such as mutual information (12) or its normalized variant (13) are used.

Another issue with high *b*-value DW-MRI concerns the remarkable change in contrast at different *b*-values and different gradient directions. At any *b*-value, the signal attenuation is orientationally variant—such that minimal signal attenuation occurs perpendicular to the long axis

[1]Department of Neurobiology, The George S. Wise Faculty of Life-Sciences, Tel Aviv University, Tel Aviv, Israel.

[2]Cardiff University Brain Research Imaging Centre (CUBRIC), School of Psychology, Cardiff University, Cardiff, United Kingdom.

[3]Neuroscience and Mental Health Research Institute, Cardiff University, Cardiff, United Kingdom.

Grant sponsor: Future and Emerging Technologies (FET) Programme within the Seventh Framework Programme for Research of the European Commission (FET-Open, "CONNECT" project); Grant number: 238292

*Correspondence to: Prof. Yaniv Assaf, Department of Neurobiology, The George S. Wise Faculty of Life Sciences, Tel Aviv University, Tel Aviv, 69978, Israel. E-mail: assafyan@post.tau.ac.il

Received 3 April 2011; revised 31 July 2011; accepted 1 August 2011.

DOI 10.1002/mrm.23186

Published online 19 Decemebr 2011 in Wiley Online Library (wileyonlinelibrary.com).

of a bundle of coherently oriented fibers and increases as the angle between the encoding vector and the long axis of the fibers increases. At high *b*-values, a residual signal remains when encoding perpendicular to the fibers, but in other orientations the signal is significantly attenuated, often reaching the noise floor (14). Consequently, the resulting DW-MRI contrast at the same *b*-value between different gradient orientations and also for the same direction with different *b*-values is not comparable. Moreover, at high *b*-values (above 3000 s/mm^2), the signal intensity is attenuated to such an extent that the edges of CSF, gray and white matter regions, and the outline of the brain are undefined. Combined, this means that image-feature based registration methods (including those that use entropy-driven cost-functions such as mutual information), will fail to correct for distortions and motion. Hence, the credibility of any inferences that are subsequently drawn from voxel-wise fitting of a model to such data decreases dramatically.

To the best of our knowledge, there has been no method published to date that allows for such images to be coregistered accurately. One possible workaround is to interleave low *b*- and high *b*-value images and correct for motion by applying the transformations derived from the low *b*-value images to the high *b*-value images that follow. However, this workaround results in longer scan duration, and it only offers indirect and incomplete motion correction—especially because the image contrast between a low and high *b*-value weighted image is so different in anisotropic tissue.

The goal of this work was to develop an image registration method that would robustly correct the motion induced misalignments and artifacts of high *b*-value DW-MR images. We suggest a framework based on both experimental data (DT-MRI) and simulations (using the CHARMED framework) to register the high *b*-value diffusion images. The proposed method can be applied to high *b*-value DW-MRI as a preprocessing registration step before any analysis.

MATERIALS AND METHODS

Subject and Image Acquisition

Sixteen healthy young subjects (20–40 years) were scanned on a 3 T (GE) MRI system in Tel Aviv Sourasky Medical Center, Israel. The protocol was approved by the local institutional review boards and all volunteers signed an informed consent. The MRI protocol included a set of echo planar diffusion-weighted images. The diffusion MRI protocol included whole brain DT-MRI and CHARMED acquisitions.

DT-MRI data were acquired along 19 unique gradient axes with a *b*-value of 1000 s/mm^2 and an additional image at $b = 0$ s/mm^2 with the following parameters: pulse repetition time/echo time = 15,000/91 ms, three averages (number of excitations), field of view = 20.2 cm, matrix size 128 × 128, giving a resolution of 1.58 × 1.58 × 2.1 mm^3. The scan time was 17 min.

CHARMED data were acquired along 34 gradient axes and additional $b = 0$ s/mm^2 in a multi b-shell acquisition with increasing number of gradient directions with the increase in *b*-value (six directions for 208 s/mm^2, 12 for 2240 s/mm^2. and 16 for 3990 s/mm^2), using the following parameters: pulse repetition time/echo time = 13,000/97 ms, $\Delta/\delta = 43/33$ ms, Gmax = 4 G/cm, field of view = 19 cm, matrix size 128 × 128, giving a resolution of 1.5 × 1.5 × 3 mm^3. The scan time was 19 min.

In the majority of the acquired datasets, the subject was instructed to remain as still as possible during the acquisition. Yet, the resulting DW-MR images were slightly-moderately misaligned due to typical subject motion, which depends on subject respiration and level of compliance/motivation.

To strictly test the ability of the suggested framework to correct for motion, we acquired a CHARMED dataset in which the subject was asked to move his head deliberately (about 10° rotations) before a nondiffusion-weighted and another 7–8 diffusion-weighted images were acquired. This was repeated four times to complete a dataset according to the gradient scheme specified above. The resulting DW-MR images were significantly misaligned due to the severe motion.

Registration and Analysis Process

The registration and analysis pipeline (Fig. 1) is designed as follows:

DT-MRI Image Analysis

The images were corrected for motion with affine (six parameters), normalized-mutual-information-based registration with respect to the $b = 0$ s/mm^2 using SPM2 with appropriate reorientation of gradient vectors (15). DT-MRI analysis was performed using in-house software to generate the diffusion tensor and common summation indices (e.g., FA).

High b-Value DW-MRI Template Simulation

Given the complete dissimilarity between images acquired with diffusion-encoding gradients along different orientations, and at different *b*-values, our method generates "template" images, derived from the low-*b*-value data, that have image contrast that matches that of a given high-*b*-value image. To do this, it was first necessary to establish how indices computed from CHARMED related to indices computed from a DT-MRI analysis. Figure 2, for example, shows that there is a strong linear relationship between the volume fraction of the restricted component (f_r), and FA, which allows one to predict f_r from FA.

Gradient direction and *b*-value specific templates for each subject were generated using the CHARMED framework (3,16). CHARMED models the diffusion signal with two diffusing components: hindered (modeled by a diffusion tensor) and restricted (modeled by diffusion within impermeable cylinders). The CHARMED framework includes several parameters: the f_r, the diffusivity and orientation of the restricted component (D_r, ϕ, and θ) and the diffusion tensor of the hindered component (D_h). In the following work, we inversely used the CHARMED model to simulate high *b*-value diffusion template images using each subject's DT-MRI data. The various DT-MRI analysis output parameters were used to

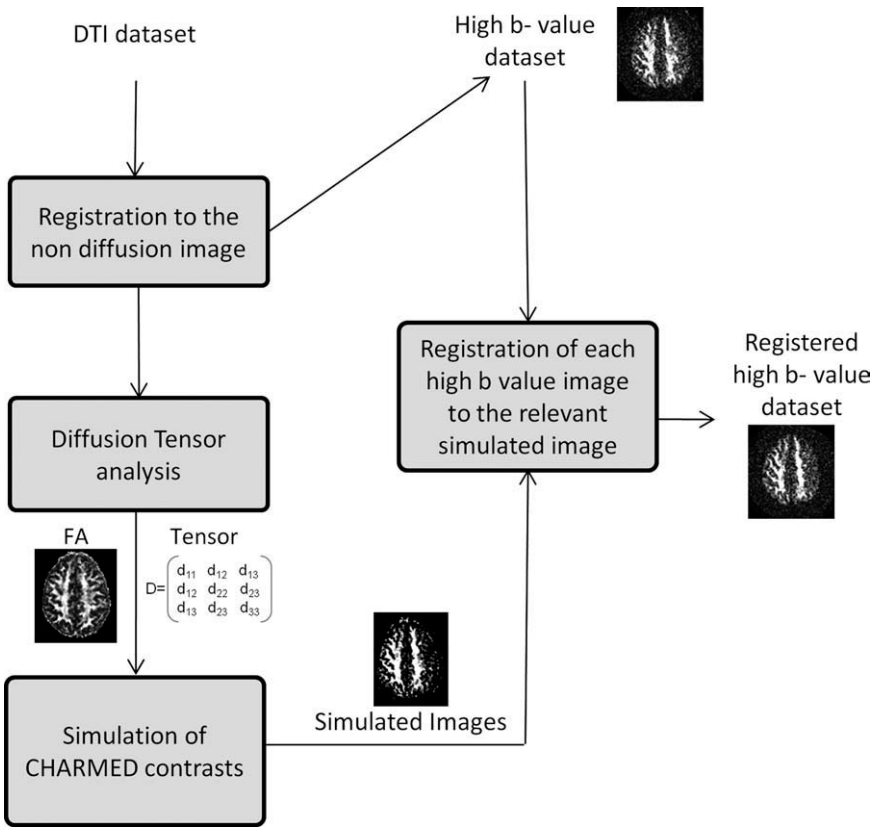

FIG. 1. Analysis routine flowchart.

estimate the CHARMED parameters for one restricted and one hindered diffusion compartments. The diffusion tensor was used to provide an estimate of D_h (mean diffusivity of the diffusion tensor), while D_r was taken as 1 $\mu m^2/ms$. f_r was predicted from FA as described above. ϕ and θ were estimated by conversion of the first eigenvector to spherical coordinates. Eq. [1] below describes the mathematical expression used for the simulation (16)

$$E_{(q,\Delta)} = f_h \cdot e^{-4\pi^2\left(\Delta-\left(\frac{\delta}{3}\right)\right)\left(|q_\perp|^2\lambda_\perp+|q_\parallel|^2\lambda_\parallel\right)} + f_r \cdot e^{-4\pi^2|q_\parallel|^2\left(\Delta-\left(\frac{\delta}{3}\right)\right)D_\parallel-(4\pi^2R^4|q_\perp|^2/D_{\perp\tau})(7/296)(2-99/112)(R^2-D_{\perp\tau})}. \quad [1]$$

This procedure yielded coregistered template images that simulated the contrast seen in diffusion weighted images acquired at different *b*-values and gradient directions in the native image space of each subject.

We Propose to Call this Method UNDISTORT (Using Nondistorted Images to Simulate a Template of the Registration Target)

Image Registration

Each acquired high *b*-value image was registered to the matching high *b*-value template (generated from the DT-MR images and the CHARMED simulation as described in the previous paragraph) using SPM2 with a global affine normalized mutual information-based registration.

Data Analysis

To demonstrate the use of the new UNDISTORT motion/distortion correction procedure, the corrected high *b*-value diffusion images were analyzed using the

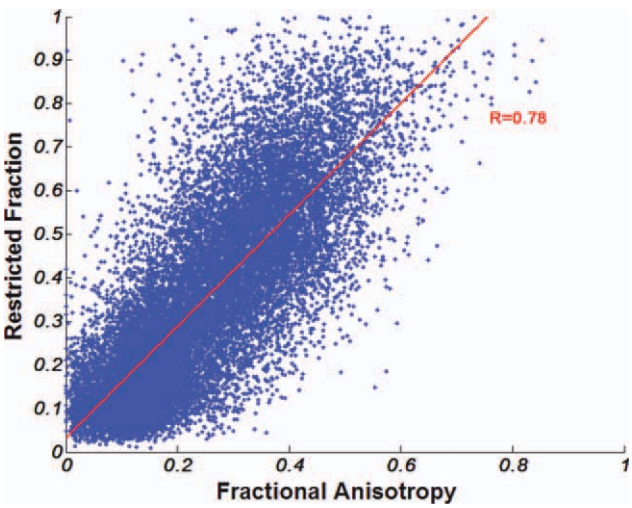

FIG. 2. The correlation between FA computed from DT-MRI and fractional restricted volume computed from CHARMED. Pearson correlation coefficient of 0.78 indicates that there is a strong linear relationship between f_r and FA, which allows one to predict f_r from FA. [Color figure can be viewed in the online issue, which is available at wileyonlinelibrary.com.]

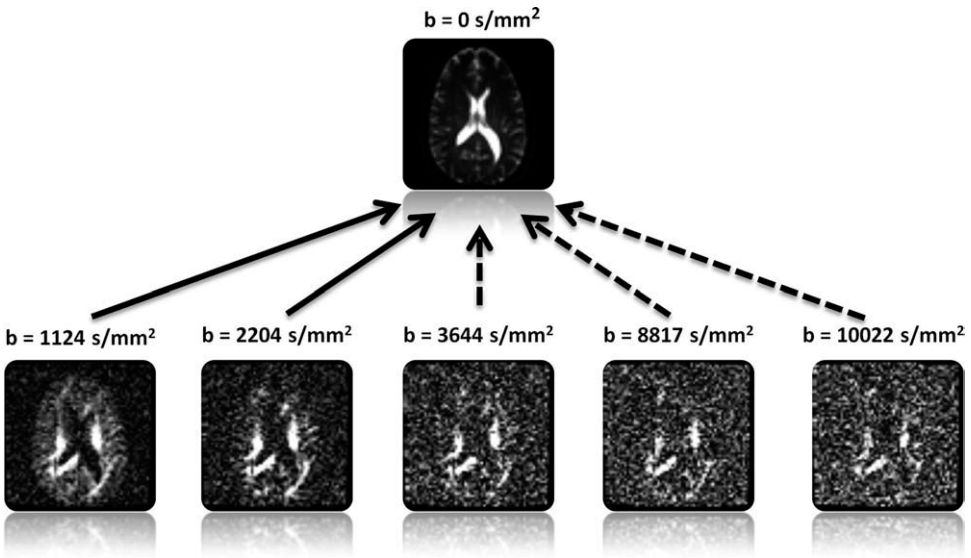

FIG. 3. Diffusion weighted data acquired with diffusion gradients applied in the same direction at different *b*-values. Note the contrast change when acquiring DW-MRIs with $b > 3000$ s/mm^2.

CHARMED framework (3). In summary, the CHARMED model was fitted using a nonlinear regression routine (using the Levenberg–Marquardt regression method) in Matlab (The Mathworks). One hindered and two restricted compartments were used to fit the registered data and the number of free parameters was 16.

Validation Methods

To establish the reliability of the UNDISTORT framework we used qualitative visual assessment of the registered DW-MR images and the fractional volume of the computed CHARMED restricted component. In addition,

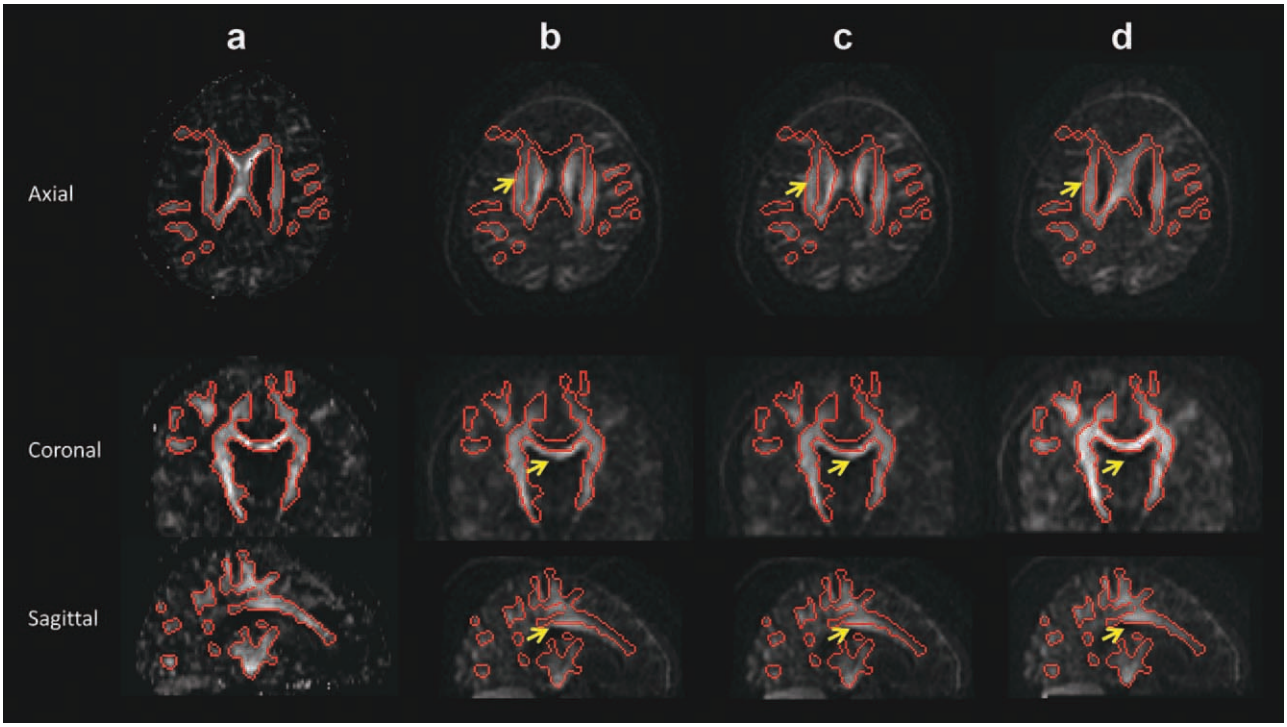

FIG. 4. A representative example for the proposed high *b*-value registration procedure. **a:** High *b*-value template image ($b = 3990$ s/mm^2, gradient direction:[−0.241, 0.931, 0.132]) compared with (**b**) the original acquisition at the same gradient direction, (**c**) the same image corrected with respect to the nondiffusion image (using SPM2 with a normalized mutual information cost-function), and (**d**) the corrected image following UNDISTORT. The outline of the white matter, as detected in the template image, was superimposed on the original and corrected images. The yellow arrows indicate regions of motion artifact in the acquired DW-MRI. Note the white matter outlined in red in the corrected volume with respect to the template image. [Color figure can be viewed in the online issue, which is available at wileyonlinelibrary.com.]

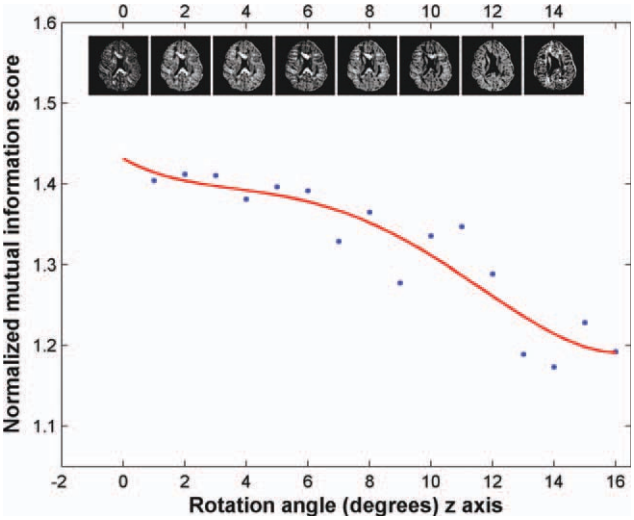

FIG. 5. Fifteen different rotation matrixes (6° around *x* axis and 1–15° around *z* axis) were applied to the tensors and 15 corresponding data sets of template images were simulated to examine the effect of the directional contrast, induced by head motion, on the template images generated in UNDISTORT. The graph shows the normalized mutual information for the different templates with respect to the nonrotated data set (blue dots), a fourth degree polynomial trendline (red line), and representative slices of the simulated template images (images on the top row) versus the rotation angle around *z* axis. Note that above 7–8° of rotation around *z* axis, the slope of the trendline rapidly decreases and the ability to simulate a matching directional contrast is notably reduced. [Color figure can be viewed in the online issue, which is available at wileyonlinelibrary.com.]

we used the residuals from the CHARMED fitting (17) to assess the quality of the fitting as an indirect measure of the quality of the motion correction. In each voxel, the error was calculated as the median of the normalized residuals calculated for all DW-MR images, i.e.,

$$E = \text{median}_k \left(\frac{|\text{DWI}^k_{\text{obs}} - \text{DWI}^k_{\text{CHARMED fit}}|}{\text{DWI}^k_{\text{obs}}} \right) \quad [2]$$

where E is the error and k is the number of analyzed DW-MR images.

In the case of minimal subject motion, residual analysis was performed for both uncorrected and template-based corrected data. However, for medium and severe motion, the uncorrected data was registered with respect to the nondiffusion image (using SPM2 with a six-parameter affine transformation) and using the suggested template-based method. Residual analysis was performed to compare the quality of the fit.

RESULTS AND DISCUSSION

Figure 3 shows a typical high *b*-value diffusion-weighted data set acquired along the same gradient direction at different *b*-values. It is evident that the image contrast is not comparable between the different *b*-values and that conventional registration method, which relies on matching the image contrast to that of the nondiffusion-weighted images, will fail.

Template Generation

Figure 4 shows a representative example for the high *b*-value registration procedure (UNDISTORT) with a high *b*-value template image (b = 3990 s/mm^2 gradient direction: [−0.241, 0.931, 0.132]) (Fig. 4a) compared with the original acquired DW-MRI (Fig. 4b) at the same gradient direction, the same image corrected with respect to the nondiffusion image (using SPM2 with a normalized mutual information cost-function) (Fig. 4c) and the corrected image following UNDISTORT (Fig. 4d). Close visual inspection of the edges of the white matter reveals that the regions outlined in red are well matched to the template image only when the UNDISTORT algorithm is

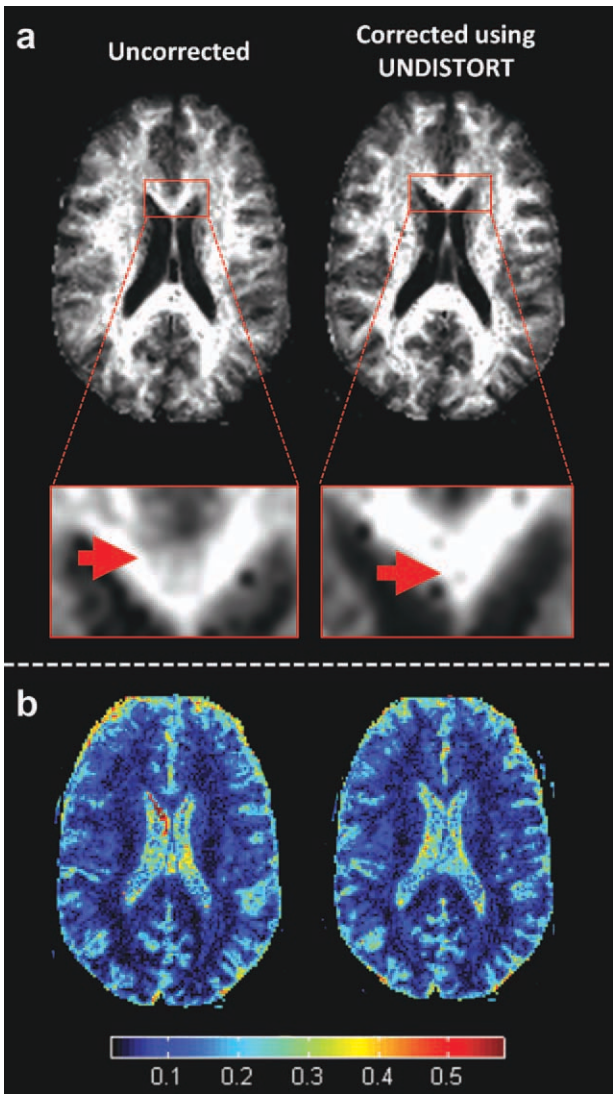

FIG. 6. Fractional restricted volume computed from CHARMED performed on the uncorrected data (left) and data corrected using UNDISTORT (right) for a subject with minimal head motion. Note the improved fitting results in the corpus callosum achieved by the suggested motion correction (**a** right) with respect to the uncorrected data (**a** left). (**b**) Residual error is mainly evident in CSF regions, thus, the reduction of the error is minor. [Color figure can be viewed in the online issue, which is available at wileyonlinelibrary.com.]

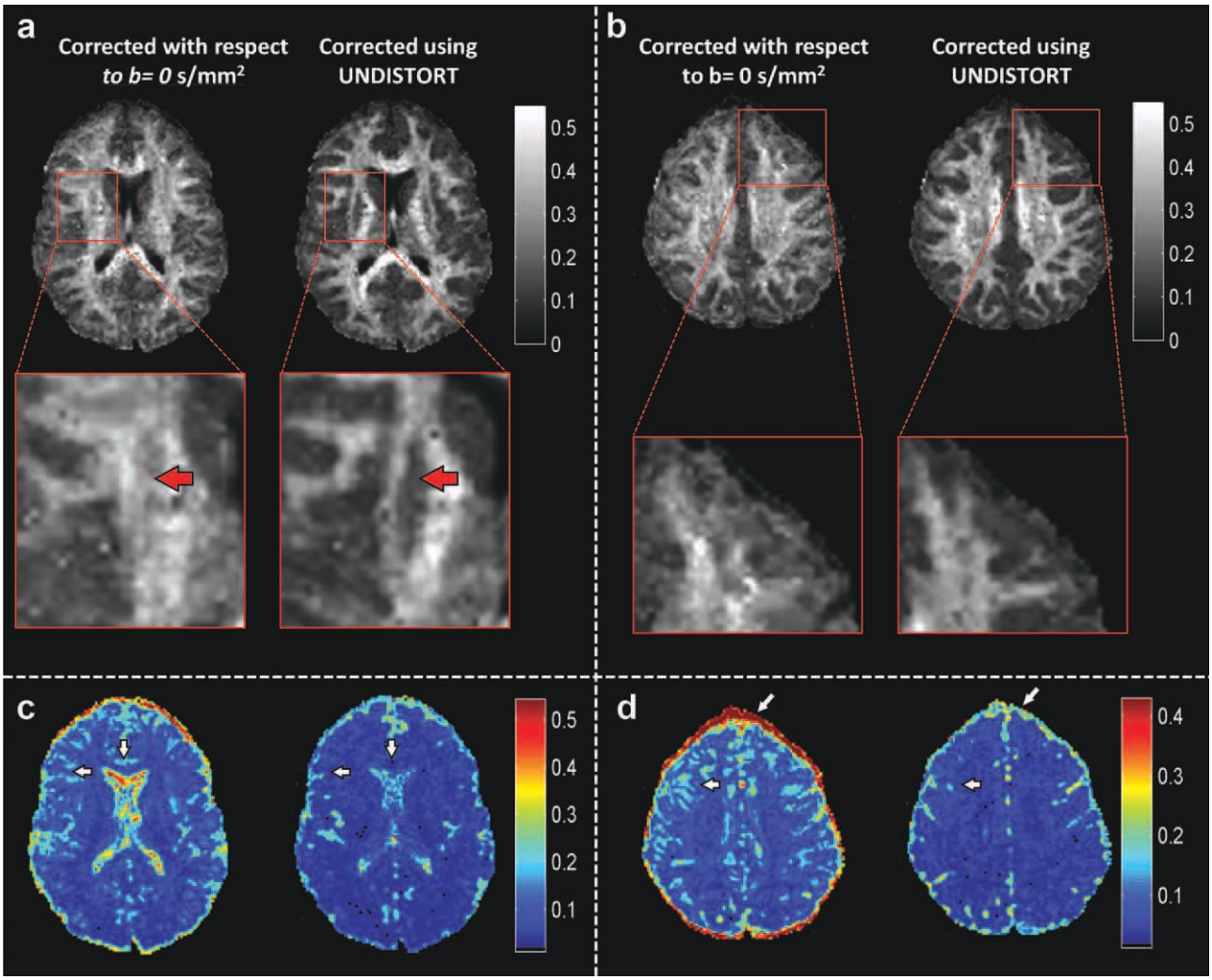

FIG. 7. Fractional restricted volume computed from CHARMED performed on data corrected with respect to the nondiffusion image (left), and the data corrected using UNDISTORT (right) for a subject with moderate head motion. Note the improved fitting results in the frontal white matter and the external and internal capsule achieved by UNDISTORT (on the right of **a,b**) with respect to the data corrected with respect to the nondiffusion image (on the left of **a,b**), respectively. The reduction in the residual error also indicates a better fit to the CHARMED model following UNDISTORT method (on the right of **c,d**) versus the data corrected with respect to the nondiffusion image (on the left of **c,d**). [Color figure can be viewed in the online issue, which is available at wileyonlinelibrary.com.]

used. It is important to note that using only one restricted component for template generation we are making a simplification of the signal in crossing fibers regions (where two or more restricted components may be required). However, we found that the contrast of the generated templates adequately matches the DW-MR image for the purposes of registration.

To examine the effect of head motion on the orientational contrast and its implication for the robustness of UNDISTORT, we selected a range of 15 rotation matrices and applied them to the tensor and to the template images. The analysis pipeline included the following steps:

Fifteen different rotations were applied to the data (6° around the *x*-axis and 1°–15° around the *z*-axis). For each of these rotations (which included appropriate reorientation of the diffusion tensor), new diffusion weighted imaging (DWI) data sets were generated and subsequently registered to the nonrotated DWI data set. DT-MRI analysis was performed on the registered DWI data sets and used to simulate 15 sets of template images, as described in the Materials and Methods. Each of the 15 data sets comprised 36 coregistered template images in which the contrast was changed according to the extent of the rotation angle and gaussian noise (variance = 0.01) was added to the noise-free template images. Finally, normalized mutual information (12) was computed for each template with respect to the nonrotated data set. Figure 5 shows how the normalized mutual information varies as a function of the angle of rotation around *z* axis. The reduction in normalized mutual information increases with rotation. When the rotation angle exceeds 7–8°, the slope of the fourth degree polynomial trendline rapidly decreases, and the ability to simulate a matching directional contrast is notably reduced.

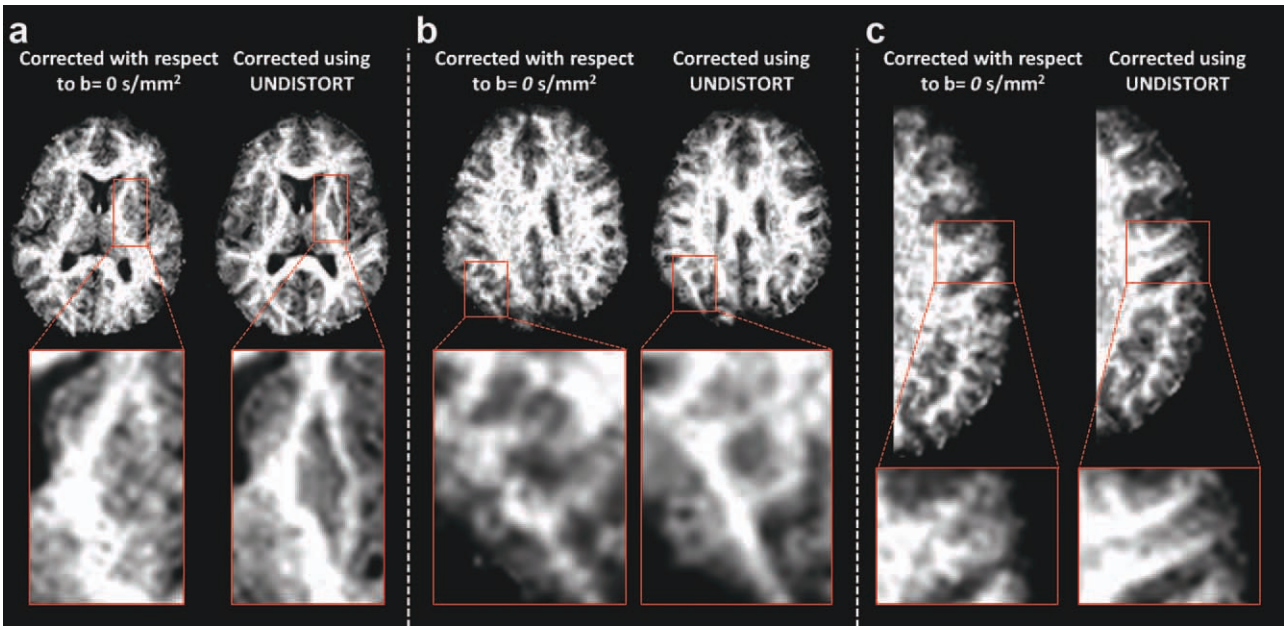

FIG. 8. CHARMED analysis for a subject with severe motion. UNDISTORT achieved better optimization (**a–c** on the right) compared with the data corrected with respect to a nondiffusion image (using SPM2 with a six-parameter affine transformation) (**a–c** on the left). Note the improved results in the external and internal capsule (**a** left versus right) and the short association fibers at the parietal lobe (**c** left versus right). [Color figure can be viewed in the online issue, which is available at wileyonlinelibrary.com.]

Minimum and Moderate Subject Motion

To demonstrate the reliability of our registration in the cases of minimum subject motion (rotations are less than 0.1° around each axis and translations of size 0.1 mm), CHARMED analysis was performed for both the uncorrected data and the template based registered data. In the cases of moderate subject motion (rotations are 1.6° around *x* axis, 0.5° around *z* axis and translations of size 4 mm in *x* axis and 4 mm in *z* axis), CHARMED analysis was performed for both the data corrected with respect to the nondiffusion image (using SPM2 with a six-parameter affine transformation and a normalized mutual information cost-function) and the template based registered data. CHARMED analysis indicated that following UNDISTORT-based motion correction, much better model fits were obtained (Figs. 6 and 7).

Residual error was used as a measure of the goodness of the fit for the uncorrected data or the data corrected with respect to the nondiffusion image versus the data corrected using UNDISTORT, where high values represent a poor fit. The residual error dramatically decreased in areas of gray and white matter when CHARMED was used to fit the data corrected using UNDISTORT in the case of moderate subject motion (Fig. 7c,d). Note the relatively large changes in the frontal and temporal lobe, the corpus callosum (Fig. 7c), and the outline of the brain (Fig. 7d).

In the subarachnoid CSF, the residual error is generally high with respect to the white and gray matter, probably due to the pulsatile flow of the CSF and its increased susceptibility for noise (14). However, before appropriate motion correction, these errors are extended to gray matter regions. As expected, the reduction in the residual error in the case of minimal subject motion following registration was less significant (Fig. 6). In the latter case, the residual error is mainly evident in the CSF, where the error remains unchanged before and after registration.

Severe Subject Motion

To further demonstrate the use of the UNDISTORT approach, in the case of severe motion (rotations are 5° around *x* axis, 8° around *z* axis and translations of size 3 mm in *x* axis and 10 mm in *z* axis), CHARMED analysis was performed for both the data registered with respect to the nondiffusion image (using SPM2 with a six-parameter affine transformation and a normalized mutual information cost-function) and the template based registered data. CHARMED analysis indicated that following template-based motion correction much better optimization was achieved (Fig. 8).

GROUP ANALYSIS

To demonstrate the benefits of using UNDISTORT, we performed CHARMED analysis for both uncorrected and corrected data using CHARMED data sets of 15 subjects acquired with the same protocol and derived the restricted volume fraction in each voxel of each subject's data set. We then normalized all calculated restricted volume fraction maps to Montreal Neurological Institute (MNI) space and computed standard deviation (SD) maps for both (corrected and uncorrected) normalized data sets. To ensure that any improvements seen in the corrected data set were not simply attributable to the smoothing introduced by the b-spline interpolation, we applied a similar interpolation to the uncorrected data

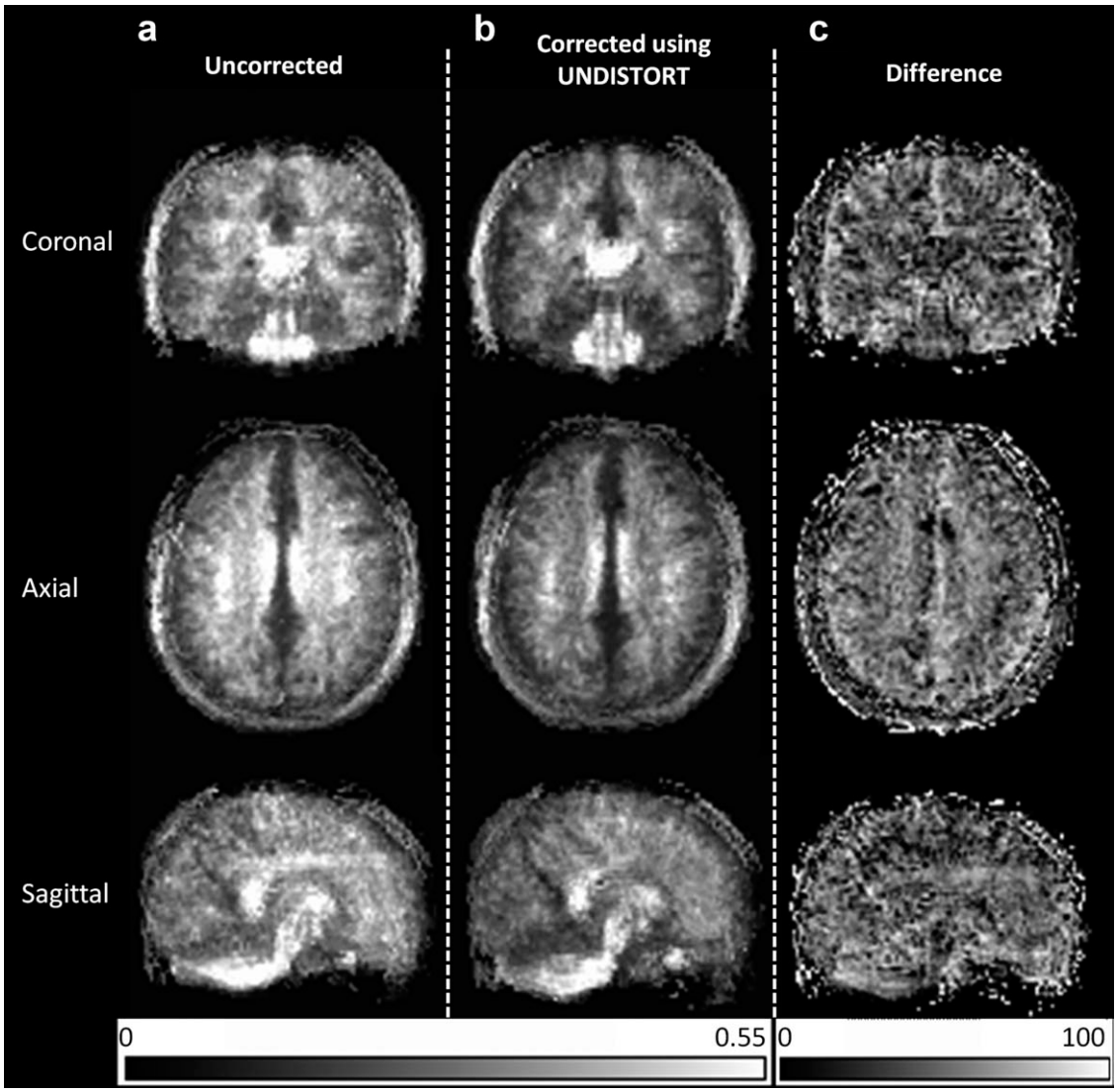

FIG. 9. SD maps of normalized f_r maps calculated for both uncorrected (**a**) and corrected using UNDISTORT (**b**) datasets of 15 subjects acquired at the same protocol. The reduction in the SD values following UNDISTORT and the uniform positivity of the difference map (**c**) indicates that UNDISTORT provides a significant improvement of CHARMED analysis results.

set before CHARMED analysis. Figure 9 shows the SD maps of normalized f_r maps calculated for both uncorrected (Fig. 9a) and UNDISTORT-corrected (Fig. 9b) data sets. The reduction in the SD values following UNDISTORT and the uniform positivity of the difference map (Fig. 9c) indicates that UNDISTORT provides a significant improvement of CHARMED analysis results.

LIMITATIONS

The orientational contrast in any diffusion-weighted image may change as a result of head motion. Thus, in the case of extreme head motion between the acquisition of the data at low *b*-values and at high *b*-values, the simulated high *b*-value contrast might be inaccurate, introducing errors in the registration (Fig. 5). However, as demonstrated in Figure 5, UNDISTORT appears to correct motion up to 7–8° of rotation. In the implementation of UNDISTORT presented here, data from a separate DT-MRI acquisition was used to generate the template data for registration of the high *b*-value data. This was because our standard CHARMED acquisition protocol only includes a small number of measurements at the low *b*-value. Having to acquire two data sets is therefore a limitation of the current implementation, however, this could be readily addressed, and the deed to acquire a separate DT-MRI data set obviated, by ensuring sufficient angular resolution at low *b*-value as part of the CHARMED acquisition. Finally, the low *b*-value data are assumed to be successfully realigned, as it is straightforward to correct it using mutual information based registration technique and the tensor fitting is assumed to be robust. However, DT-MRI may suffer from many pitfalls (18) and if there are errors (misregistration, etc.) in the estimate of the tensor, they will affect the simulated signal and impact on the performance of UNDISTORT.

CONCLUSION

We have presented a novel framework for correcting image distortion and patient motion of high *b*-value diffusion-weighted images. We used the diffusion tensor, the first eigenvector and the FA maps computed by the DT-MRI, and the CHARMED model to generate simulated high *b*-value images. The UNDISTORT procedure yields a set of coregistered template images, wherein each image can be used as a reference image for the registration of a matching high *b*-value image. In the absence of a gold standard for the registration of high *b*-value DW-MRI, the CHARMED model was used to estimate the validity of the suggested framework. Both qualitative and quantitative results demonstrated an improvement in fitting the data to the CHARMED model following the template-based registration.

This new approach addresses a long-standing problem and makes correction of motion and distortion in data collected at high *b*-values feasible for the first time. This will open an opportunity to explore and compare the abilities of the different high *b*-value approaches in tissue characterization and disease diagnosis.

ACKNOWLEDGMENTS

The authors thank Shir Hofstetter, Ido Tavor, and Silvia De-Santis for providing data and helpful discussions.

REFERENCES

1. Assaf Y, Mayk A, Cohen Y. Displacement imaging of spinal cord using q-space diffusion-weighted MRI. Magn Reson Med 2000;44:713–722.
2. Seo HS, Chang KH, Na DG, Kwon BJ, Lee DH. High *b*-value diffusion ($b = 3000$ s/mm2) MR imaging in cerebral gliomas at 3T: visual and quantitative comparisons with $b = 1000$ s/mm2. AJNR Am J Neuroradiol 2008;29:458–463.
3. Assaf Y, Basser PJ. Composite hindered and restricted model of diffusion (CHARMED) MR imaging of the human brain. Neuroimage 2005;27:48–58.
4. Assaf Y, Ben-Bashat D, Chapman J, Peled S, Biton IE, Kafri M, Segev Y, Hendler T, Korczyn AD, Graif M, Cohen Y. High *b*-value q-space analyzed diffusion-weighted MRI: application to multiple sclerosis. Magn Reson Med 2002;47:115–126.
5. Basser PJ. Inferring microstructural features and the physiological state of tissues from diffusion-weighted images. NMR Biomed 1995;8:333–344.
6. Assaf Y, Pasternak O. Diffusion Tensor Imaging (DTI)-based White Matter Mapping in Brain Research: A Review. J Mol Neurosci 2008;34:51–61.
7. Jones DK. Diffusion MRI: theory, methods, and application, Vol.xvi. New York: Oxford University Press. 2011; 767p.
8. Pierpaoli C, Jezzard P, Basser PJ, Barnett A, Di Chiro G. Diffusion tensor MR imaging of the human brain. Radiology 1996;201:637–648.
9. Cohen Y, Assaf Y. High *b*-value q-space analyzed diffusion-weighted MRS and MRI in neuronal tissues—a technical review. NMR Biomed 2002;15:516–542.
10. Tuch DS, Reese TG, Wiegell MR, Wedeen VJ. Diffusion MRI of complex neural architecture. Neuron 2003;40:885–895.
11. Wu YC, Alexander AL. Hybrid diffusion imaging. Neuroimage 2007;36:617–629.
12. Studholme C, Hill DLG, Hawkes DJ. An overlap invariant entropy measure of 3D medical image alignment. Pattern Recogn 1999;32:71–86.
13. Haselgrove JC, Moore JR. Correction for distortion of echo-planar images used to calculate the apparent diffusion coefficient. Magn Reson Med 1996;36:960–964.
14. Jones DK, Basser PJ. "Squashing peanuts and smashing pumpkins": how noise distorts diffusion-weighted MR data. Magn Reson Med 2004;52:979–993.
15. Leemans A, Jones DK. The B-matrix must be rotated when correcting for subject motion in DTI data. Magn Reson Med 2009;61:1336–1349.
16. Assaf Y, Freidlin RZ, Rohde GK, Basser PJ. New modeling and experimental framework to characterize hindered and restricted water diffusion in brain white matter. Magn Reson Med 2004;52:965–978.
17. Andersson JL, Skare S. A model-based method for retrospective correction of geometric distortions in diffusion-weighted EPI. Neuroimage 2002;16:177–199.
18. Jones DK, Cercignani M. Twenty-five pitfalls in the analysis of diffusion MRI data. NMR Biomed 2010;23:803–820.